Int. J. Electrochem. Sci., 14 **(2019)** 10270 – 10280, doi: 10.20964/2019.11.28

International Journal of
ELECTROCHEMICAL
SCIENCE
www.electrochemsci.org

Excellent Electrochemical Performance of Multilayer Graphite Nanosheets as an Anode Material for Lithium-Ion Batteries

Qiuju Lu[1,2,3], *Peichao Lian*[1,2,3,*], *Qian Wang*[1,2,3], *Zefu Zuo*[1,2,3], *Yi Mei*[1,2,3,*]

[1] Faculty of Chemical Engineering, Kunming University of Science and Technology, Kunming 650500, China
[2] Yunnan Provincial Key Laboratory of Energy Saving in Phosphorus Chemical Engineering and New Phosphorus-based Materials
[3] The Higher Educational Key Laboratory for Phosphorus Chemical Engineering of Yunnan Province, Kunming 650500, China
[*]E-mail: lianpeichao@kmust.edu.cn; meiyi412@126.com

Received: 6 July 2019 / *Accepted:* 23 August 2019 / *Published:* 7 October 2019

Graphite anodes occupy a considerable share of the commercial market of lithium-ion batteries (LIBs) due to their appropriate potential profile and low cost. Nevertheless, this type of anode material is far from enough to meet the increasing demands of electronic devices and hybrid electric vehicles (HEVs) due to its relatively low lithium storage capacity (372 mAh g^{-1} at LiC_6). Graphene is a one-atom-thick layer of graphite that exhibits a larger reversible capacity than that of graphite but large voltage hysteresis and poor cycling performance during charge and discharge processes. Herein, multilayer graphite nanosheets (few-layer graphene) were prepared by using a facile and efficient high-pressure homogenizer method. The as-prepared multilayer graphite nanosheets were used as an anode material for LIBs and exhibited good cycling stability and rate performance. After 50 cycles, the material still retained a high reversible capacity of 573 mAh g^{-1} at a current density of 100 mA g^{-1}. Even at a high current density of 1000 mA g^{-1}, the reversible specific capacity of the prepared multilayer graphite nanosheets is still as high as 510 mAh g^{-1}. More importantly, the multilayer graphite nanosheets have no obvious voltage hysteresis.

Keywords: Multilayer graphite nanosheets; High-pressure homogenizer method; Anode materials; Lithium-ion batteries

1. INTRODUCTION

Lithium-ion batteries (LIBs) have been used as the leading power source for portable electronics because of their relatively high energy density, long lifespan, lack of memory effect and environmental friendliness [1-3]. The energy density and performance of LIBs largely depend on the physical and chemical properties of the cathode and anode materials [4]. The possibilities for the

improvement of cathode materials are quite limited due to the stringent requirements, such as high potential, structural stability, and inclusion of lithium in the structure [5, 6]. In recent years, various anode material candidates for LIBs have been extensively studied [7-9]. Although Si-based (P-based, Sn-based, Ge-based) composites [10-15] and metal compounds (oxides, phosphides, nitrides) [16-18] possess excellent lithium storage properties, their poor stability makes them inadequate for practical applications. By contrast, carbon-based materials are still the most common option for the anode [19]. Since the pioneering work of SONY in 1990, graphitic materials spread extensively as commercial anode materials because of their flat potential profile versus lithium and their structural stability during cycling [20, 22]. Nevertheless, the relatively low lithium storage capacity (372 mAh g^{-1} for the intercalation compound of LiC_6) cannot meet the increasing demands for electronic devices and recently developed hybrid electric vehicles (HEVs).

Graphene is a one-atom-thick layer of graphite [22]. Since the first report on the lithium storage properties of graphene as a high-capacity anode material for rechargeable lithium secondary batteries (LIB) by EunJoo Yoo et al. [23], graphene has been considered as a potential alternative to graphite because the former has a larger reversible capacity, but it should be noted that graphene sheet electrodes exhibit a large voltage hysteresis between the charge and discharge voltage curves [24, 25]. In addition, the cycling performance of the graphene anode is not satisfactory. Therefore, it is necessary and important to explore a novel graphite-based material for improving the electrochemical performance.

In this study, multilayer graphite nanosheets were prepared via a facile high-pressure homogenization (HPH) process. The electrochemical performance of multilayer graphite nanosheet anodes for LIBs was evaluated in coin-type cells. The multilayer graphite nanosheets have high reversible lithium storage capacity and good cycling stability but no obvious voltage hysteresis.

2. EXPERIMENTAL

2.1 Synthesis of multilayer graphite nanosheets

A typical sample was prepared by dispersing 400 mg graphite powder (Shanghai Colloid Chemical Factory, China) in the desired sodium dodecyl sulfate (SDS, Tianjin Fengchuan Chemical Reagent Factory, China) solution at a concentration of 0.4 mg mL^{-1} using a low-power sonic bath (Branson 1510E-MT bath sonicator) for 1 h. The homogeneous dispersion was passing through a high-pressure homogenizer (AH-BASIC, ATS Engineering Inc., Shanghai), and the pressure in the inlet was controlled to be 100 MPa by adjusting the valve gap; then, the resultant solution was centrifuged to remove unexfoliated graphite. Next, the supernatant was filtered through a polytetrafluoroethylene (PTFE) membrane. Finally, the obtained product was dried naturally for subsequent testing.

2.2. Materials characterization

The morphology and structure of the as-prepared specimens were investigated by scanning electron microscopy (SEM, TESCAN, VEGA-3SBH). The crystal structure of the obtained product

was characterized by powder X-ray diffraction (XRD, Bruker D8 Advance) using a Cu Ka source at a scanning speed of 5°min^{-1}. To analyze the quality of the sample, Raman spectra excited by 532 nm lasers were recorded on a LabRAM HR Evolution spectrometer.

2.3. Electrochemical measurements

The electrochemical performance of the multilayer graphite nanosheets was evaluated using CR2032 coin-type cells. The multilayer graphite nanosheets were mixed with carbon black and polyvinylidene fluoride (PVDF) binder in N-methyl-2-pyrrolidone (NMP) to form a homogeneous slurry at a weight ratio of 70:20:10. Then, the slurry was coated on the copper foil using a doctor blade and dried at 100 °C under vacuum for 2 h. The foil was then punched into small pieces with a diameter of 14 mm. To test the electrochemical performance under different current densities, the multilayer graphite nanosheet electrodes were assembled in an argon-filled glove box with lithium foil as the counter and reference electrode and glass fibers as the separator. The electrolyte was composed of $LiPF_6$ (1 mol L^{-1}) in a mixture of ethylene carbonate (EC) and diethyl carbonate (DEC) (1:1 by volume). The galvanostatic charge/discharge tests were performed using a Neware battery testing system with a voltage window ranging from 0.01 to 3.0 V versus Li/Li^+ at 100 mA g^{-1}.

3. RESULTS AND DISCUSSION

3.1 Preparation and microstructure characterization of multilayer graphite nanosheets

A schematic illustration of the preparation process of the multilayer graphite nanosheets through a HPH method is illustrated in Fig. 1. The process occurs in a homogenization valve comprising an impact ring and a valve seat. The suspension was pumped through a nozzle and released into an expansion chamber. During the process, the van der Waals-like forces between graphite layers were weakened by two types of mechanical force: normal force (changing the interlayer distance) and lateral force (sliding away) [26], so this method can exfoliate graphite efficiently and quickly. Compared with the conventional sonication method, the HPH process takes less time and can efficiently exfoliate graphite into multilayer graphite nanosheets.

SEM and TEM were used to characterize the structure of the graphite and the multilayer graphite nanosheet materials. Fig. 2 shows the morphologies of the natural graphite and the multilayer graphite nanosheets. Fig. 2a and b show the SEM images of the initial graphite, revealing a flaky and compact structure. Fig. 2c and d show the SEM images of the multilayer graphite nanosheets; a curled morphology, consisting of a thin wrinkled paper-like structure, can be observed from the SEM images. It is obvious that the stacking of nanosheets is substantially disordered and that the nanosheets are agglomerated and overlapped, revealing that most of the graphite has been efficiently exfoliated into multilayer nanosheets. The thickness of the multilayer graphite nanosheets can be observed from the TEM images (Fig. 2e and f). It was found that the multilayer graphite nanosheet thickness ranged from 10 to 50 nm, which is thicker than graphene reported in the literature [27-29]. Therefore, we have

successfully prepared multilayer graphite nanosheets by using a high-pressure homogenizer, and their thickness is between that of graphite and graphene.

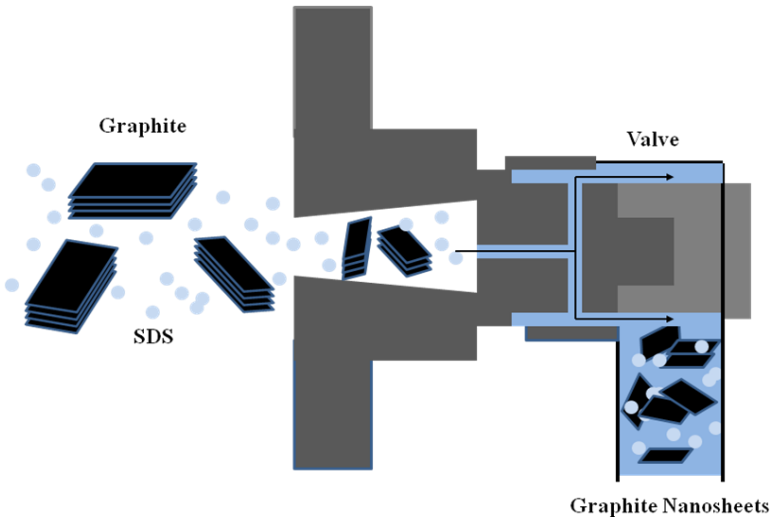

Figure 1. Schematic illustration of the preparation process of multilayer graphite nanosheets.

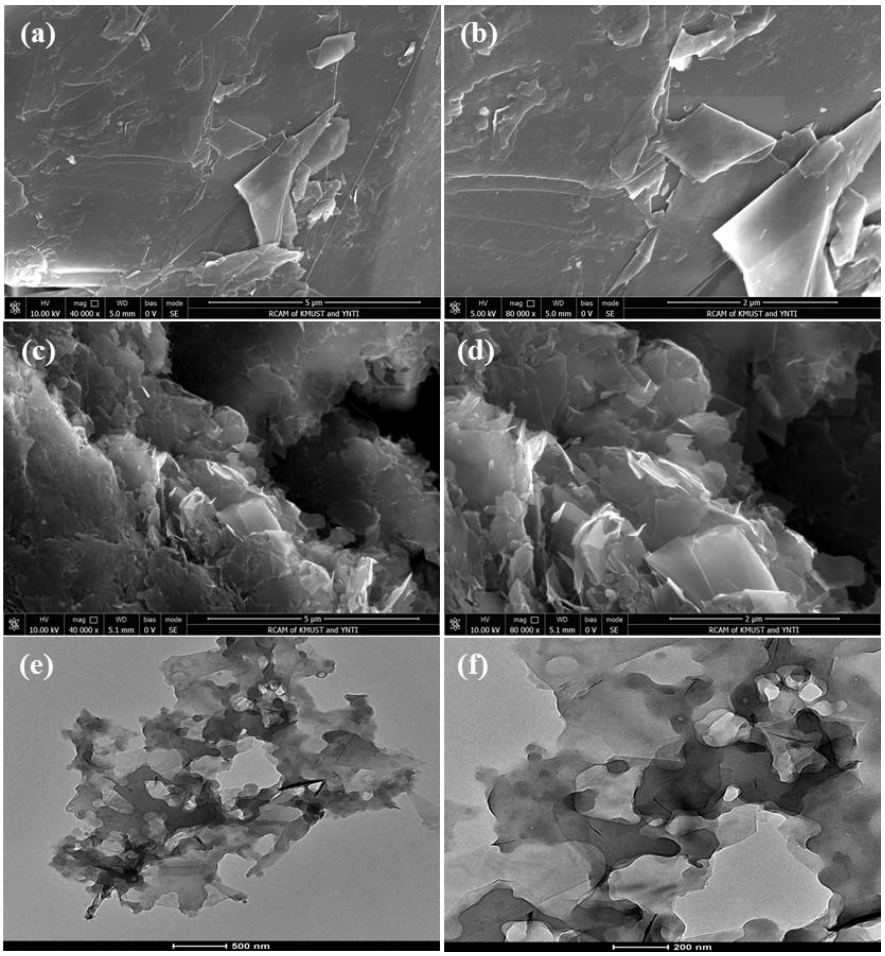

Figure 2. SEM images of (a, b) initial graphite, (c, d) graphite nanosheets and TEM images of (e, f) graphite nanosheets.

The X-ray diffraction (XRD) patterns of the natural graphite and the multilayer graphite nanosheets are shown in Fig. 3. As shown in Fig. 2a, the natural graphite exhibits high crystallinity, which is in accordance with the peaks established by JCPDS Card No. 41-1487. From Fig. 2b, compared with the natural graphite, the multilayer graphite nanosheets display only two very weak diffraction peaks; the intensities of the (002) and (004) peaks were greatly weakened, while the (100), (102) and (103) peaks disappeared, indicating that the crystallinity of the multilayer graphite nanosheets is very poor and that the graphite has successfully been exfoliated into multilayer graphite nanosheets. This observation is consistent with the results of SEM and TEM mentioned above.

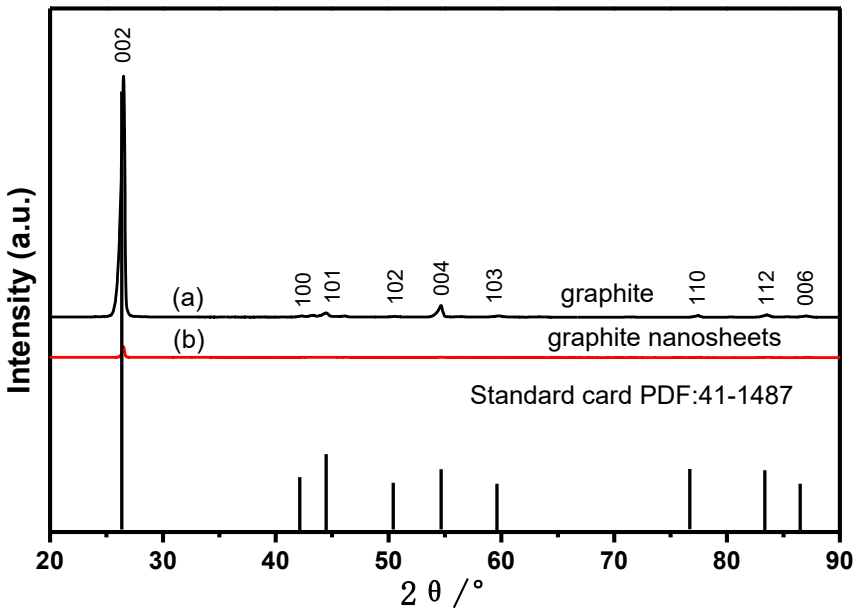

Figure 3. XRD patterns of (a) the initial graphite and (b) the multilayer graphite nanosheets.

Significant structural changes occurring during the HPH process from graphite to the multilayer graphite nanosheets can also be characterized by Raman spectroscopy. As shown in Fig. 4, three characteristic peaks of the multilayer graphite nanosheets can be easily distinguished in the Raman spectra. The D mode of the multilayer graphite nanosheets is caused by the breathing mode of the sp^2 carbon atoms, which is attributed to the κ-point phonons of A_{1g} symmetry. The D peak reflects the degree of disorder of the material [30]. As a significant difference, the D mode of the multilayer graphite nanosheets is stronger than that of the natural graphite, indicating the introduction of edge or basal plane defects and suggesting that the graphite has been successfully stripped into disordered multilayer graphite nanosheets. It should be pointed out that a similar phenomenon of the appearance of edge defects during the liquid exfoliation process has been reported [31, 32]. The Raman spectrum of the graphite, as expected, displays a prominent G peak at 1574 cm^{-1}, corresponding to first-order scattering of the E2g mode [33]. In the Raman spectrum of the multilayer graphite nanosheets, the G band is shifted to 1583 cm^{-1}. In contrast, the 2D band has nothing to do with the G peak but is attributed to the second order of zone-boundary phonons [34]. The Raman spectrum of the multilayer

graphite nanosheets shows a similar trend in shape and intensity of the 2D peak compared to that of the initial graphite. It has been reported that when graphene is less than 5 layers thick, the shape and position of its 2D peak are significantly different from those of graphite [34]. Therefore, the thickness of the multilayer graphite nanosheets is greater than five layers, which is consistent with the results observed by TEM and SEM. In addition, the multilayer graphite nanosheets show an apparently higher I_D/I_G (0.35 for the multilayer graphite nanosheets) than that of the initial graphite (0.029), which suggests that the multilayer graphite nanosheets are more disordered than the initial graphite. The significant increase in the D/G intensity ratio compared to that of highly crystalline graphite indicated a decrease in the size of the in-plane sp^2 domains and a partially disordered crystal structure of the graphite nanosheets [35], as indicated by the XRD analysis.

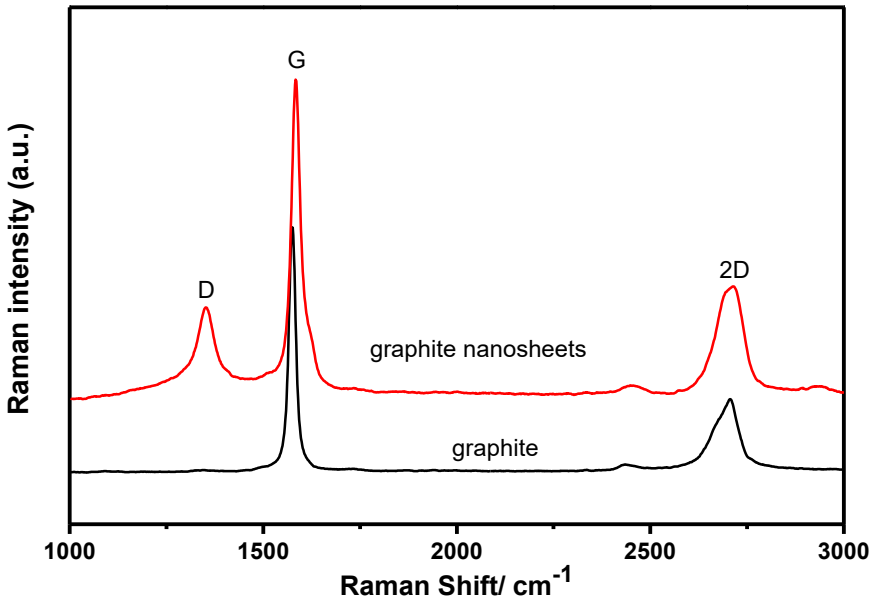

Figure 4. Raman spectra of the initial graphite and the multilayer graphite nanosheets.

3.2 Electrochemical performance of the multilayer graphite nanosheets

The electrochemical performance of the multilayer graphite nanosheets as an anode material for LIBs was evaluated via a galvanostatic charge-discharge test in the potential range from 0.01 to 3.0 V at 100 mA g^{-1}. The discharge/charge profiles of the multilayer graphite nanosheet anodes in the 1st, 2nd, 5th, 10th and 50th cycles are shown in Fig. 5a. During the first cycle, the discharge and charge capacities of the multilayer graphite nanosheets are 857 and 566 mAh g^{-1}, respectively, which are higher than the first discharge and charge capacities of graphite-based materials reported previously [36-39] (see Table 1). The reason for the increase in specific capacity may be attributed to the reduced number of layers and the defects of the multilayer graphite nanosheets compared to graphite. The irreversible capacity loss can be attributed to the generation of the solid electrolyte interface (SEI) layer in the first cycle [40]. In subsequent cycles, the discharge/charge curves gradually overlap,

suggesting that the multilayer graphite nanosheets possess stable cycling performance. During the discharge process, the slope of the curve starts from 3.0 V, and the large part of the specific capacity (>70%) falls in the region below 0.5 V [25]. It is obvious that the first discharge curve exhibits a plateau at approximately 0.7 V, representing the formation of the SEI layer. In each charge process, a long voltage plateau at approximately 0.2 V is observed. More interestingly, the shape of the discharge/charge curves of the multilayer graphite nanosheets especially matches well with that of graphite [24], indicating that the multilayer graphite nanosheets have no obvious voltage hysteresis.

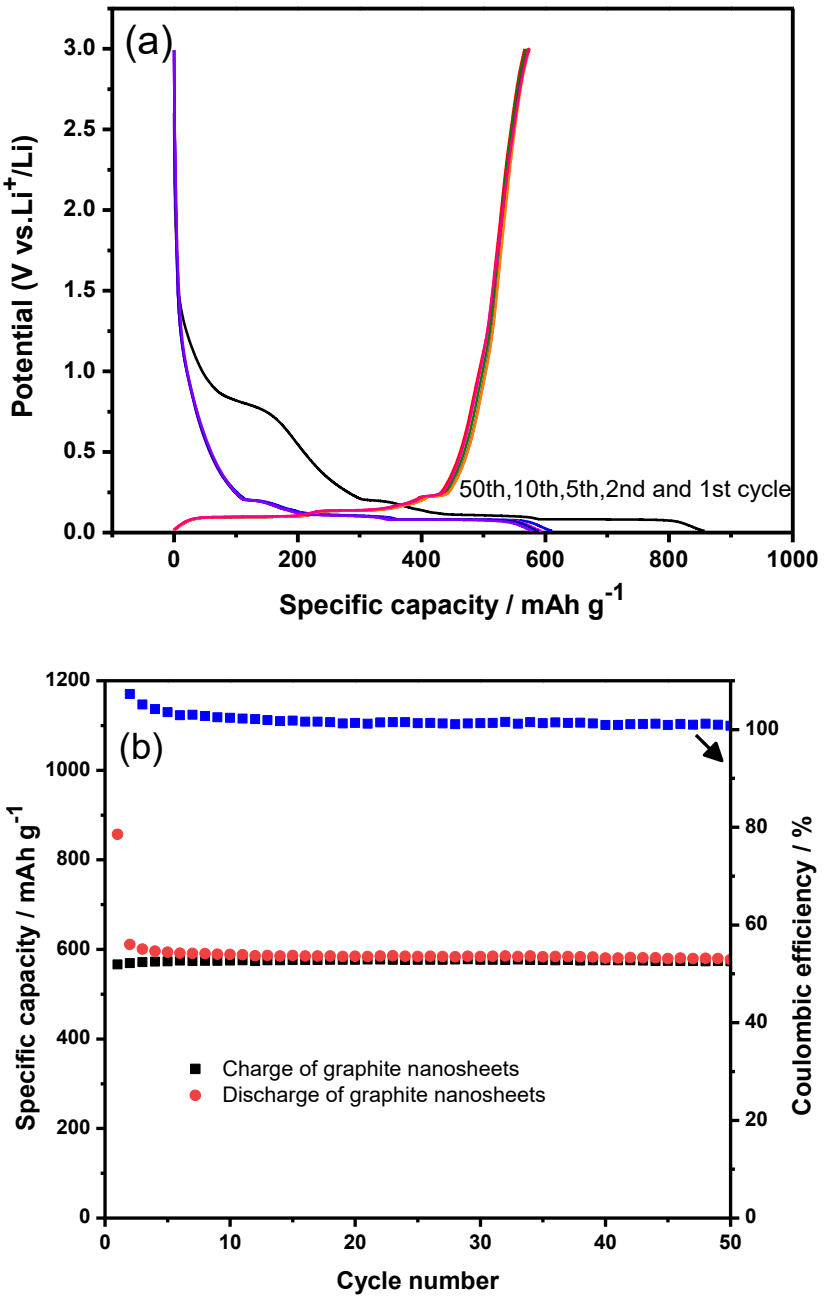

Figure 5. (a) Voltage profiles of the multilayer graphite nanosheets at 100 mA g^{-1}, (b) Cycling performance and coulombic efficiency of the multilayer graphite nanosheets at 100 mA g^{-1}.

Table 1. The capacities of different graphite-based materials

Anode materials	*First discharge capacity (mAh g^{-1})*	*First charge capacity (mAh g^{-1})*	*Reversible capacity for the 50th cycle (mAh g^{-1})*	*Capacity retention at the 50th cycle (%)*	*Reference*
KOH etched graphite	363	335	268	74	36
Highly oriented pyrolytic graphite	439	363	346	79	37
Spherical natural flake graphite	360	304	259	72	38
Graphite-grafted silicon	489	382	361	74	39
Multilayer graphite nanosheets	857	566	573	98	This work

The cycling performance and coulombic efficiency of the multilayer graphite nanosheets were examined under long-term cycling over 50 cycles, demonstrating a good cyclic performance and high coulombic efficiency (as shown in Fig. 5b). After 50 cycles, the multilayer graphite nanosheet anode still maintained a specific capacity of 573 mAh g^{-1}, showing better cycling performance than that of other reported graphite-based materials [36-39] (see Table 1). The increase in capacity can be attributed to the activation process of the material [41]. Based on the above results, the multilayer graphite nanosheets have a high reversible lithium storage capacity and good cycling stability but no obvious voltage hysteresis.

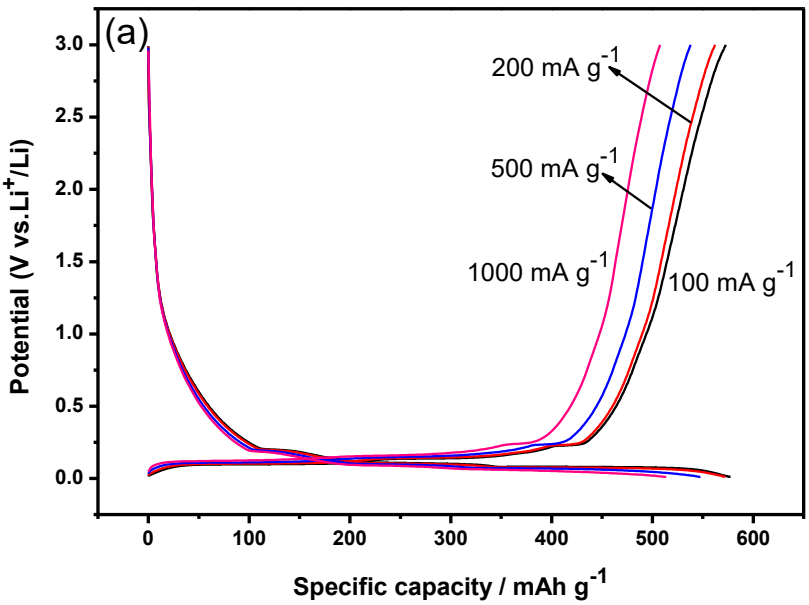

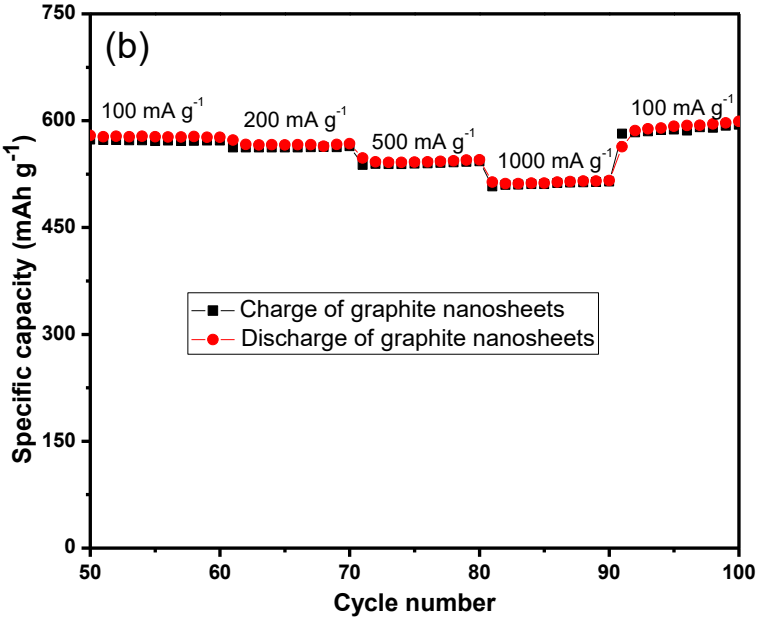

Figure 6. (a) Discharge/charge curves of multilayer graphite nanosheets at various specific currents of 100 mA g^{-1} (52nd cycle of cycling test, 2nd cycle at 100 mA g^{-1}), 200 mA g^{-1} (62nd cycle of cycling test, 2nd cycle at 200 mA g^{-1}), 500 mA g^{-1} (72nd cycle of cycling test, 2nd cycle at 500 mA g^{-1}), and 1000 mA g^{-1} (82nd cycle of cycling test, 2nd cycle at 1000 mA g^{-1}); (b) Cycling performance of multilayer graphite nanosheets at 100, 200, 500, and 1000 mA g^{-1}.

The rate performance of the multilayer graphite nanosheets was also investigated. As depicted in Fig. 6a and b, the multilayer graphite nanosheets demonstrate good rate capability at current rates ranging from 100 mA g^{-1} to 1000 mA g^{-1} between the voltages of 0.01 and 3.0 V. Under current densities of 100, 200, and 500 mA g^{-1}, the multilayer graphite nanosheets retain capacities of 573 mAh g^{-1}, 562 mAh g^{-1}, and 539 mAh g^{-1}, respectively. Even at a high current density of 1000 mA g^{-1}, the multilayer graphite nanosheets still maintain a capacity of 510 mAh g^{-1} with almost no decay, suggesting outstanding rate performance. More attractively, when the current density was restored to 100 mA g^{-1} after 90 cycles at various current densities, a reversible specific capacity of 583 mAh g^{-1} remained in the 100th cycle. These results indicate that multilayer graphite nanosheets show great potential as candidate anode materials for lithium-ion batteries with high reversible capacity, outstanding cycling performance and high-rate charge/discharge properties.

4. CONCLUSIONS

In summary, multilayer graphite nanosheets were successfully prepared by using a facile and efficient high-pressure homogenizer method. The prepared multilayer graphite nanosheets have thicknesses ranging from 10 nm to 50 nm. The electrochemical measurements suggested that the multilayer graphite nanosheets exhibited high reversible capacity and good cycle performance when used as an anode material for lithium-ion batteries. More importantly, the multilayer graphite nanosheets have no obvious voltage hysteresis. The abovementioned excellent properties are perhaps because the thickness of the multilayer graphite nanosheets is larger than that of graphene and the

degree of defects is greater than that of graphite. The results reported in this manuscript will provide a new strategy for improving the electrochemical performance of graphite-based electrode materials for lithium-ion batteries. Moreover, the strategy of improving the electrochemical performance by regulating the number of layers of graphite will lay the foundation for the design of high-performance layered electrode materials for lithium-ion batteries.

ACKNOWLEDGMENTS
This work was financially supported by the Yunnan Yunling Scholar Cultivation Fund (10978195), Natural Science Foundation of China (21968012), Yunnan Talent Reserve Project (2015HB022), and Yunnan Natural Science Foundation (2016FB018).

References

1. B. Huang, X. Li, Y. Pei, S. Li, X. Cao, R.C. Massé and G. Cao, *Small*, 12 (2016) 1945.
2. S. Zhu, J. Li, X. Deng, C. He, E. Liu and F. He, *Adv. Funct. Mater.*, 27 (2017) 1605017.
3. L. Lu, X. Han, J. Li and J. Hua, *J. Power Sources*, 226 (2016) 272.
4. G. Qu, J. Wang, G. Liu, B. Tian and C. Su, *Adv. Funct. Mater.*, 29 (2019) 1805227.
5. G. Wang, X. Shen, J. Yao and J. Park, *Carbon*, 47 (2009) 2049.
6. M. Wakihara, *Mater. Sci. Eng., A*, 33 (2001) 109.
7. M.S. Whittingham, *Chem. Rev. (Washington, DC, U. S.)*, 104 (2004) 4271.
8. R. Marom, S.F. Amalraj, N. Leifer and D. Jacob, *J. Mater. Chem.*, 21 (2011) 9938.
9. M. Armand and J.M. Tarascon, *Nature*, 451 (2008) 652.
10. Y. Dong, Z.S. Wu, W. Ren, H.M. Cheng and X. Bao, *Sci. Bull.*, 62 (2017) 724.
11. Q. Wang, P. Lian, B. Wang, Y. Tang, H. Liu and Y. Mei, *Ionics*, 24 (2018) 3393.
12. P. Lian, J. Wang, D. Cai, G. Liu and Y. Wang, *J. Alloys Compd.*, 604 (2014) 188.
13. D.J. Xue, S. Xin, Y. Yan, K.C. Jiang and Y.X. Yin, *J. Am. Chem. Soc*, 134 (2012) 2512.
14. H. Xiang, K. Zhang, G. Ji, J.Y. Lee, C. Zou, X. Chen and J. Wu, *Carbon*, 49 (2011) 1787.
15. Z. Yu, B. Tian, Y. Li, D. Fan, D. Yang and G. Zhu, *ACS Appl. Mater. Interfaces*, 11 (2018) 534.
16. X. Wang, H.M. Kim, Y. Xiao and Y.K. Sun, *J. Mater. Chem. A*, 4 (2016) 14915.
17. P. Lian, J. Wang, D. Cai, L. Ding, Q. Jia and H. Wang, *Electrochim. Acta*, 116 (2014) 103.
18. M.S. Balogun, M. Yu, C. Li, T. Zhai, Y. Liu and X. Lu, *J. Mater. Chem. A*, 2 (2014) 10825.
19. N.A. Kaskhedikar and J. Maier, *Adv. Mater. (Weinheim, Ger.)*, 21 (2009) 2664.
20. R. Yazami, *Electrochim. Acta*, 45 (1999) 87.
21. K. Chang and W. Chen, *ACS Nano*, 5 (2011) 4720.
22. K.S. Novoselov, D. Jiang and F. Schedin, *Natl. Acad. Sci. USA*, 102 (2005) 10451.
23. E.J. Yoo, J. Kim, E. Hosono, H. Zhou, T. Kudo and I. Honma, *Nano Lett.*, 8 (2008) 2277.
24. P. Lian, X. Zhu, S. Liang, Z. Li, W. Yang and H. Wang, *Electrochim. Acta*, 55 (2010) 3909.
25. G. Wang, X. Shen, J. Yao and J. Park, *Carbon*, 47 (2009) 2049.
26. Y. Arao, Y. Mizuno, K. Araki and M. Kubouchi, *Carbon*, 102 (2016) 330.
27. Z.S. Wu, W. Ren, L. Wen, L. Gao, J. Zhao and Z. Chen, *ACS Nano*, 4 (2010) 3187.
28. C. Lee, X. Wei, J.W. Kysar and J. Hone, *Science (Washington, DC, U. S.)*, 321 (2008) 385.
29. K. Chang and W. Chen, *J. Mater. Chem.*, 21 (2011) 17175.
30. A.C. Ferrari and J. Robertson, *Phys. Rev. B: Condens. Matter Mater. Phys.*, 61 (2000) 14095.
31. Y. Hernandez, V. Nicolosi, M. Lotya and F.M. Blighe, *Nat. Nanotechnol.*, 3 (2008) 563.
32. K.R. Paton, E. Varrla, C. Backes, R.J. Smith and U. Khan, *Nat. Mater.*, 13 (2014) 624.
33. F. Tuinstra and J.L. Koenig, *J. Chem. Phys.*, 53 (1970) 1126.
34. A.C. Ferrari, J.C. Meyer, V. Scardaci and C. Casiraghi, *Phys. Rev. Lett.*, 97 (2006) 187401.

35. G. Wang, J. Yang, J. Park, X. Gou and B. Wang, *J. Phys. Chem. C*, 112 (2008) 8192.
36. Q. Cheng, R. Yuge, K. Nakahara, N. Tamura and S. Miyamoto, *J. Power Sources*, 284 (2015) 258.
37. S.K. Jeong, M. Inaba, R. Mogi, Y. Iriyama, T. Abe and Z. Ogumi, *Langmuir*, 17 (2001) 8281.
38. L. Zou, F. Kang, Y.P. Zheng and W. Shen, *Electrochim. Acta*, 54 (2009) 3930.
39. C. Martin, M. Alias, F. Christien, O. Crosnier, D. Bélanger and T. Brousse, *Adv. Mater. (Weinheim, Ger.)*, 21 (2009) 4735.
40. P. Guo, H. Song and X. Chen, *Electrochem. Commun.*, 11 (2009) 1320.
41. P. Kun, F. Wéber and C. Balázsi, *Cent Eur J Chem.*, 9 (2011) 47.